# Effects of thermal treatment on structural, optical and electrical properties of NiO thin films

Shadrach T. Akinkuade[a,b,*], Walter E. Meyer[a], Jacqueline M. Nel[a]

[a]*Physics Department, University of Pretoria, Pretoria, 0002, South Africa*
[b]*Physics Unit, Science Technology Department, Federal Polytechnic, Ado-Ekiti, Nigeria*

## Abstract

The spin-coating technique was utilized to produce thin films of nickel oxide on glass substrates. Three drying temperatures, 160 °C, and 200 °C, and 250 °C were used. Annealing temperatures ranged from 300 °C to 600 °C. The effects of drying and annealing temperatures on the films were examined with X-ray diffraction, scanning electron microscopy, Raman spectroscopy, UV-vis spectrophotometry and linear four-point probe measurements. The crystallinity of the films was found to improve as the annealing temperature increased. The average crystallite size varied from 14 nm to 28 nm for films that were dried at 200 °C and 14 nm to 32 nm for films that were dried at 250 °C as the annealing temperature was increased. Optical transmittance of the films from 800 nm to 350 nm, varied from 64% and 96%. Two peaks at 558 cm$^{-1}$ and 1100 cm$^{-1}$ in the Raman spectra of the films confirmed the presence of NiO on the films.

*Keywords:*

Nickel oxide, Annealing, Sol-gel, Spin coating, Resistivity

## 1. Introduction

Nickel oxide (NiO) is a transition metal oxide, it has a wide optical band gap from 3.6 to 4.0 eV [1] that crystallizes in the cubic rock-salt structure [2]. In stoichiometric form, NiO is an insulator, with a resistivity of about $10^{13}$ Ω.cm [3, 4] and can not be used as a

---

*Corresponding author
Email address:* `u14302552@tuks.co.za` (Shadrach T. Akinkuade)

semiconductor. P-type conductivity in NiO has been attributed to nickel vacancies or oxygen interstitials [5]. Due to interesting properties of nickel oxide such as chemical stability, wide and tunable optical band gap, and p-type conductivity, it has been found useful in many applications such as electrochromic displays [6], p-type conducting oxide [1], active layer in chemical sensors [7], solar cells [8, 9, 10], ultra violet detectors [11, 12], light emitting diodes [13] and photoelectrolysis [14].

Many techniques have been employed to produce NiO thin films including electron beam evaporation [15], sputtering [16], thermal evaporation [17], pulsed laser deposition [18], spin-coating [19], dip-coating [20, 21], chemical bath deposition [22], and spray pyrolysis [23]. The properties of these films that make them suitable for specific applications depend on conditions and techniques of deposition [24]. Simplicity, low cost, and ease of control of the microstructure of the deposited film are some of the gains of the sol-gel technique [25].

In the production of thin films of nickel oxide, hydrated nickel acetate is a common precursor, 2-methoxy ethanol is used as a solvent while monoethanolamine serves as the stabilizer. The films are usually subjected to two thermal processes during fabrication; drying to evaporate organic solvents and annealing for the transformation of precursor or any intermediate product formed during drying into NiO. Thermal decomposition of hydrated metal acetates takes place in three steps in different temperature regions [26, 27], reports on the effects of different processing temperatures on the electrical properties of sol-gel fabricated NiO films is scarce in literature. For instance, Al-Ghamdi *et al* [19] studied the structural and optical properties of NiO films (excluding resistivity) dried at $200\,^{\circ}\text{C}$ and annealed at $600\,^{\circ}\text{C}$. Jlassi *et al* [20] dried NiO films at $275\,^{\circ}\text{C}$ and annealed the films at temperatures from $300\,^{\circ}\text{C}$ to $600\,^{\circ}\text{C}$, $600\,^{\circ}\text{C}$ was found to be the optimum temperature of annealing and the study was focused on the effects of number of layers and annealing atmosphere on the properties of the films annealed at this temperature. The effects of lithium doping on the properties of NiO films dried at $300\,^{\circ}\text{C}$ and annealed at $600\,^{\circ}\text{C}$ was studied by Sta *et al* [28]. In this work, the effects of different temperatures of drying and annealing on some properties of NiO thin films were investigated.

## 2. Experimental

Microscope slides made of soda lime glass were used as substrates. Before deposition, they were cut into 25 mm × 10 mm × 1mm and washed as described elsewhere [29]. 0.75 M solution of nickel (II) acetate tetrahydrate (Ni(CH$_3$COO)$_2$.4H$_2$O) was prepared in 2-methoxy ethanol (C$_3$H$_8$O$_2$). Monoethanolamine (C$_2$H$_7$NO) (MEA) was used as the stabilizer. The molar ratio of nickel acetate to MEA was 1.0. Stirring of the solution was done for 60 minutes at 65 °C, the solution was allowed to age for 24 hours at the room temperature.

The prepared solution was spin coated onto the washed substrates at 3000 rpm for 25 s. Drying of the films was done for 10 minutes at 160 °C, 200 °C and 250 °C. The process was repeated four times. The films were annealed for 1 hour in air inside a tube furnace between 300 °C and 600 °C.

Structural properties of the films were studied with a Rigaku Smartlab X-ray diffractometer (XRD) using Cu K$\alpha$ radiation ($\lambda$ = 0.15409 nm) in the range of 2$\theta$ from 5 ° to 89.9 °. The morphology of the films was studied with field emission scanning electron microscope (FESEM ZEISS Crossbeam 540) at an acceleration voltage of 1 kV while a Bruker Dimension Icon scanning probe microscope (SPM) in ScanAsyst mode was used to examine the topography of the films. The transmittance spectra were recorded with a CARY 100 BIO UV-vis spectrophotometer in the wavelength range 200 nm to 800 nm. Raman spectra were recorded between 300 and 1500 cm$^{-1}$ using WITec alpha300 RAS+ confocal Raman microscope, with 532 nm excitation laser at 50 mW laser power. The resistivity of the samples was obtained using the linear four-point probe measurement system.

## 3. Results and discussion

### 3.1. Structural properties

#### 3.1.1. X-ray diffraction

The XRD patterns of the films are presented in Figure 1. The peaks at 37.24 °, 43.23 ° and 62.85 ° originating from diffraction planes (111), (200) and (220) were indexed to NiO (JCPDS card number 47-1049) [30]. The XRD results showed the polycrystalline nature

of the face-centred NiO films with no preferred orientation. The interplanar distance and lattice parameter for each plane of diffraction was calculated, the average lattice constant of the film was found to be 0.4180 nm which was very close to 0.4178 nm of JCPDS 47-1049. The film that was dried at 160 °C, annealed at 300 °C (the XRD pattern not shown) was amorphous. The intensities of XRD peaks for other films dried at this temperature were generally low when compared to XRD peaks of other films dried at higher temperatures. The intensities did not show a remarkable increase with an increase in annealing temperatures, this might be due to the fact that the stabilizer (MEA) has a boiling point of 170.8 °C. Therefore, it does not vaporize at 160 °C and phase transformation from precursor to NiO did not take place.

The intensity of diffraction peaks of films that were dried at 200 °C and 250 °C increased with annealing temperature. This shows that high annealing temperatures favor the transformation from precursor to NiO. The maximum intensity of peaks was observed in the film dried at 200 °C. Above this drying temperature, there might be rapid vaporization of solvent and stabilizer during the drying process which could hinder crystallization of NiO. The full-width-half-maximum (FWHM) of the films were perceived to decrease with annealing temperature. Crystallite size of the films that were dried at 200 °C and 250 °C were calculated based on the FWHM of the peaks (111), (200) and (220) using the Scherrer formula [31], the result is shown in Table 1. The crystallite size was found to increase as the temperature of annealing increased. The drying temperature was found to have less of influence on the crystallite size.
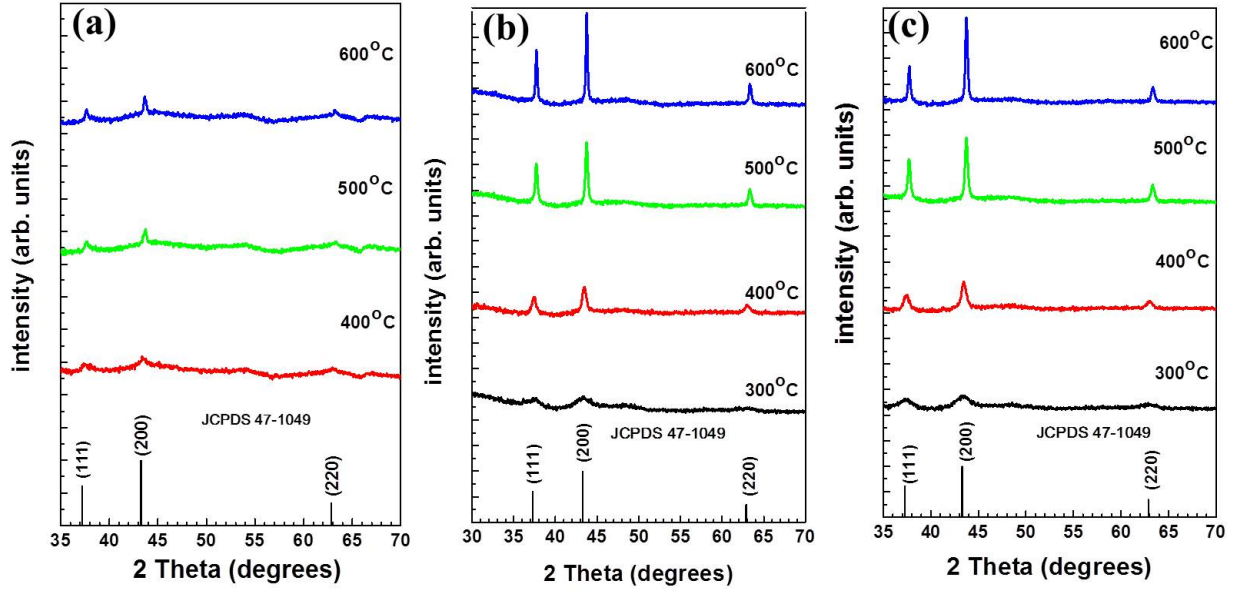
Figure 1: XRD patterns of films dried at (a) $160\,^{\circ}$C (b) $200\,^{\circ}$C and (c) $250\,^{\circ}$C.

Table 1: Summary of some features of the films

| Drying temperature (°C) | Annealing temperature (°C) | Average crystallite size (mm) | Optical Band gap (eV) | Resistivity (Ω.cm) |
|---|---|---|---|---|
| | 400 | - | 3.94 | 210 |
| 160 | 500 | - | 3.92 | 135 |
| | 600 | - | 3.87 | 820 |
| | 400 | 13.64 | 3.71 | 186 |
| 200 | 500 | 16.31 | 3.64 | 125 |
| | 600 | 28.39 | 3.55 | 770 |
| | 400 | 13.40 | 3.79 | 170 |
| 250 | 500 | 24.56 | 3.76 | 105 |
| | 600 | 31.70 | 3.74 | 670 |

### 3.1.2. Microstructural properties

The scanning electron micrographs of the thin films are presented in Figure 2. The images revealed that the films were granular, with grains of uniform size, there was an increase in grain size as the annealing temperature is raised. This is in agreement with the XRD results. Details of the grains can be observed more distinctly in the SEM images of films that were annealed at $500\,°\text{C}$ and $600\,°\text{C}$. The SPM micrographs ($1\mu\text{m} \times 1\mu\text{m}$) of the films that were dried at $250\,°\text{C}$ and annealed at different temperatures are shown in Figure 3. The root-mean-square values of the surface roughness of these films were obtained as 1.58 nm, 2.77 nm and 4.93 nm respectively.

**Annealed at 300ºC**   **Annealed at 400ºC**   **Annealed at 500ºC**   **Annealed at 600ºC**

**Dried at 160ºC**

(a) 500 nm  (b) 500 nm  (c) 500 nm  (d) 500 nm

**Dried at 200ºC**

(e) 500 nm  (f) 500 nm  (g) 500 nm  (h) 500 nm

**Dried at 250ºC**

(i) 500 μm  (j) 500 nm  (k) 500 nm  (l) 500 nm
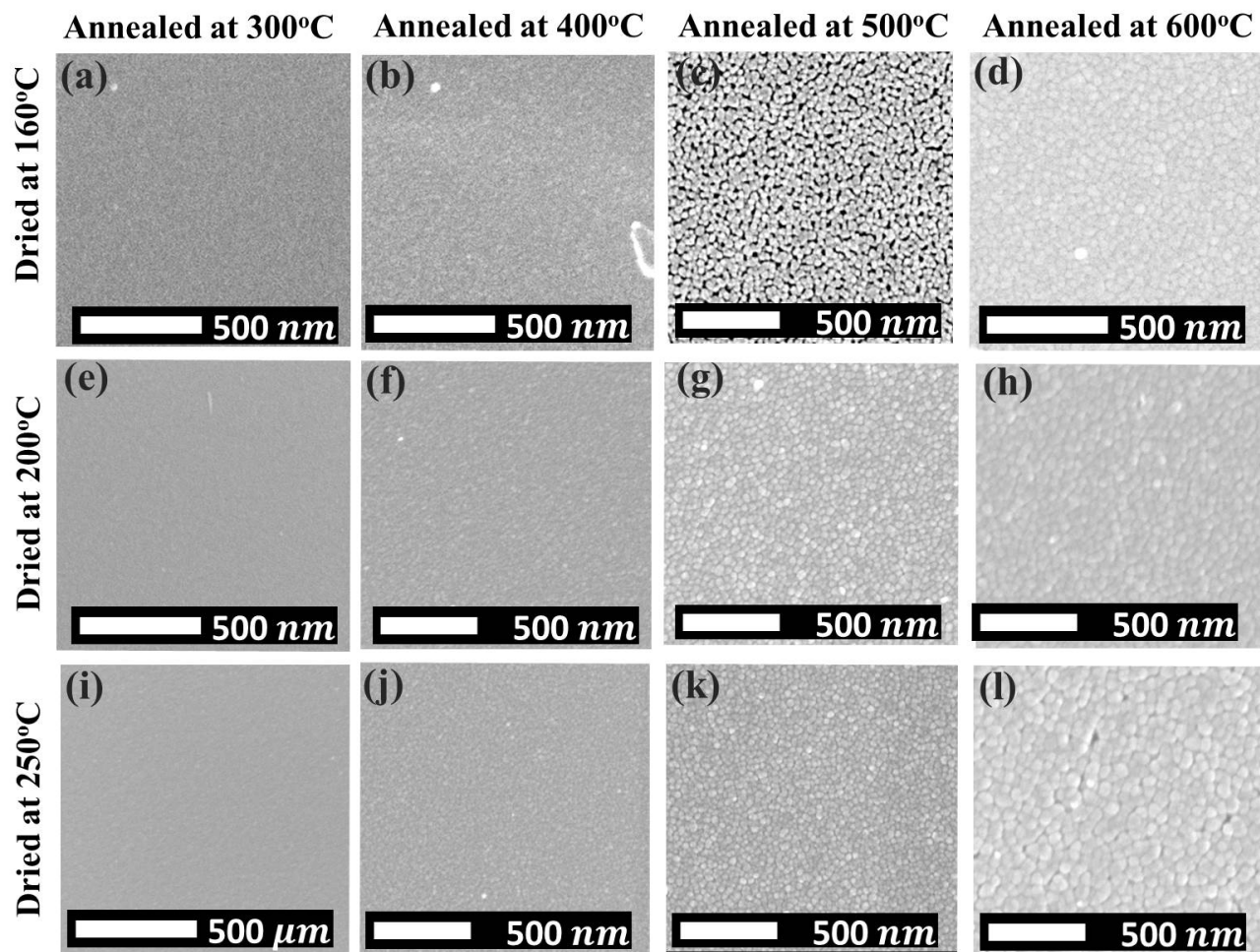
Figure 2: FESEM images of films dried at 160 °C, 200 °C, 250 °C annealed at 300 °C, 400 °C, 500 °C and 600 °C.
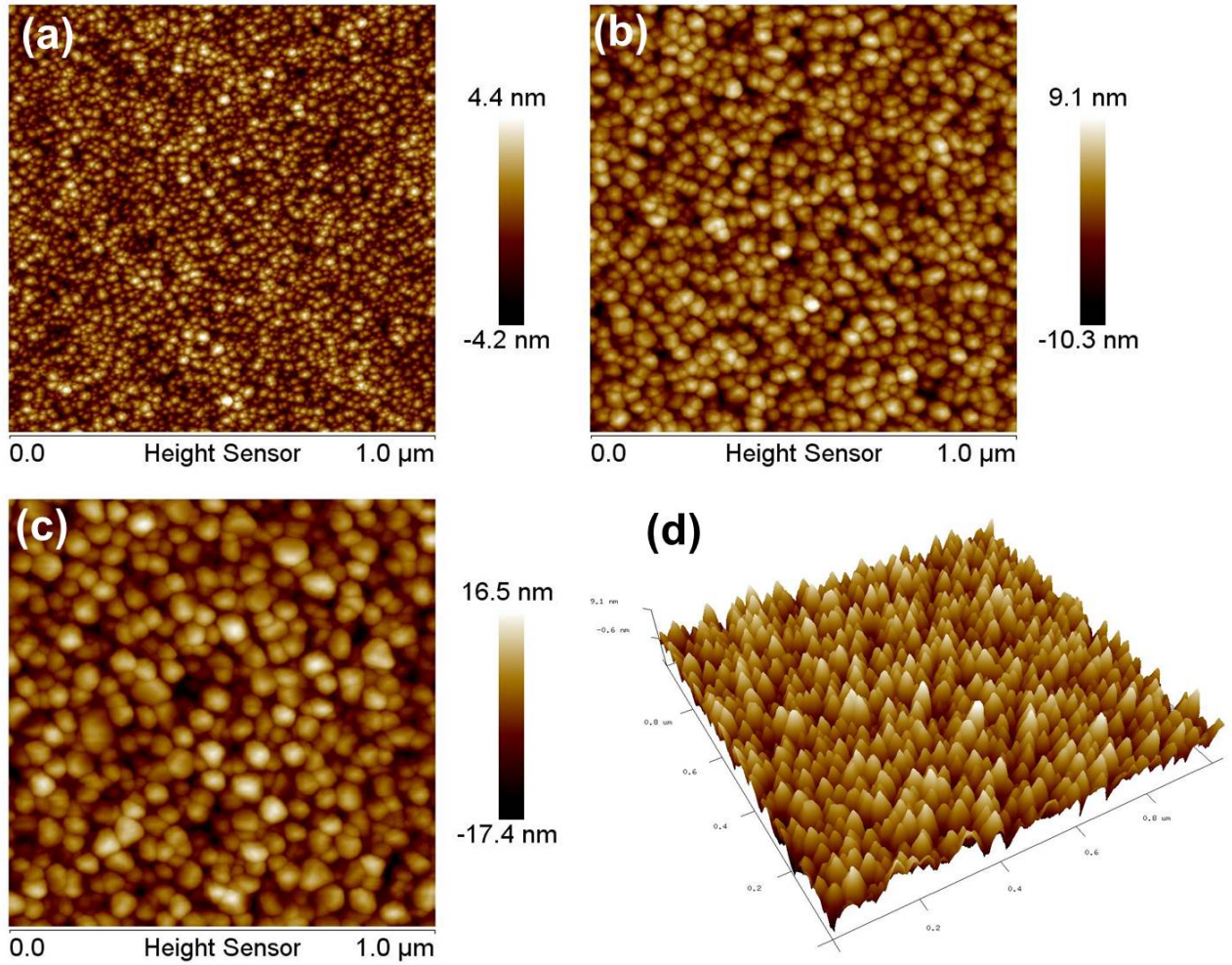
Figure 3: SPM image of films dried at 250 °C, annealed at (a) 400 °C , (b) 500 °C, (c) 600 °C and (d) 3-D image (1$\mu$m ×1$\mu$m) of film annealed at 500 °C.

## 3.2. Optical properties

### 3.2.1. Raman spectroscopic analysis

Figure 4 shows the Raman spectra of the films recorded from 300 cm$^{-1}$ to 1500 cm$^{-1}$. The spectra have two bands, these were among the five bands of vibrational origin in NiO as stated by [32]. There were two prominent peaks around 560 cm$^{-1}$ and 1100 cm$^{-1}$, in the spectra of the films that were dried at 160 °C. These were one-phonon first-order longitudinal-optical (1P) LO mode and two-phonon second-order longitudinal-optical mode (2P) 2LO respectively. For films that were dried at 200 °C and 250 °C, the intensity of the

(2P) 2LO peak (1100 cm$^{-1}$) varies with annealing temperature. The increase in the intensity of (1P) LO peak in NiO was due to parity-breaking defects such as nickel vacancies [32], thus the increase in the peak at 557 cm$^{-1}$ in the spectra of films dried at 200 °C, annealed at 400 °C and films dried at 250 °C and annealed at 400 °C and 500 °C, suggest that these films could have nickel vacancies as defects.
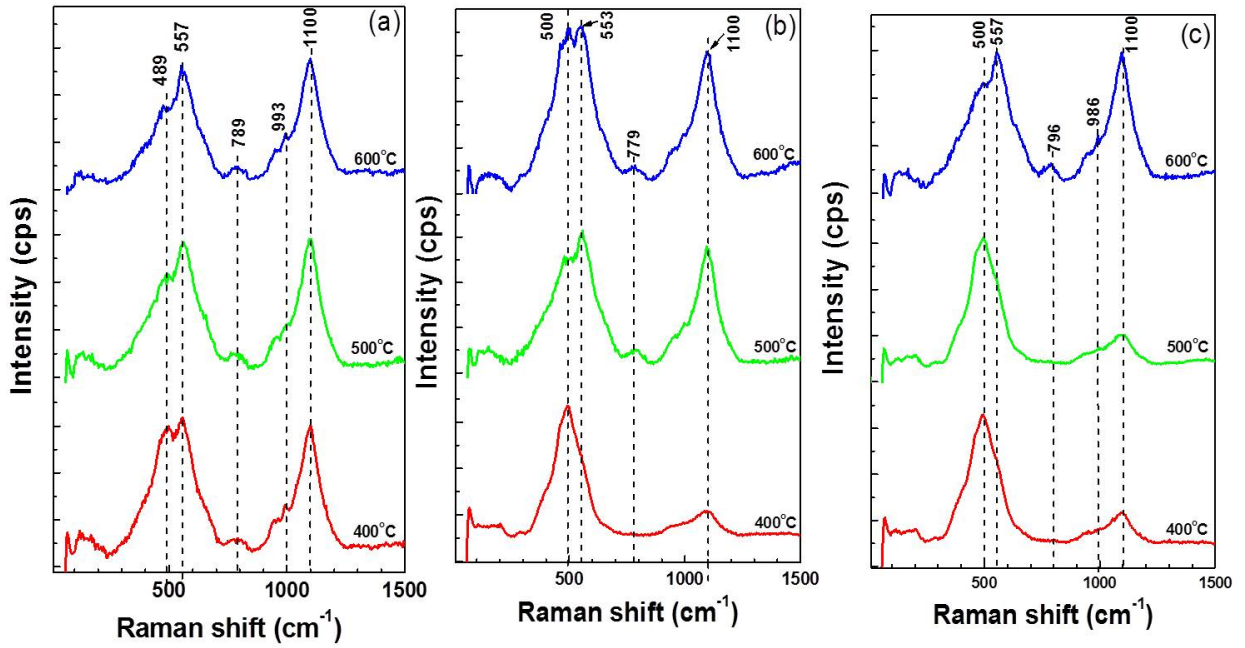


Figure 4: Raman spectrum of films (a) dried at 160 °C (b) dried at 200 °C (c) dried at 250 °C and annealed between 400 °C and 600 °C.

## 3.2.2. UV-vis spectrophotometric analysis

The transmittance spectra as measured from 300 to 800 nm are given in Figure 5. From 800 nm to 350 nm, the transmittance of films that were dried at 160 °C varied from 96% to 78%. For films that were dried at 200 °C, transmittance varied from 87% to 64% while transmittance in films that were dried at 250 °C varied from 92% to 72%. The lower transmittance observed in the films that were dried 200 °C, might be ascribed to increase in the scattering of photons in the films due to increasing grain size compared to films dried at 160 °C. There were ripples in the transmittance spectra of films dried at 200 °C and 250 °C, this was due to interference between light and nanoparticles in the films [33] or interference

among multiple reflected waves [34].

The coefficient of absorption was calculated from $\alpha = \frac{1}{d} ln \frac{1}{T}$ [15], where $T$ is the transmittance and $d$ is the film's thickness. The optical band gap $E_g$ of the film was obtained from the plot of $(\alpha h v)^2$ versus photon energy $(hv)$, as explained by [15], where $h$ is the Plank's constant. The calculated optical band gaps are stated in Table 1. The decrease in the optical band gaps of these films due to the rise in annealing temperatures might be caused by quantum confinement. According to Sing *et al* [35], the band gap of a nanomaterial varies inversely to the diameter of its nanoparticles. The increase in the annealing temperature results in an increase in the size of particles, consequently, the optical band gap of the films decreases.
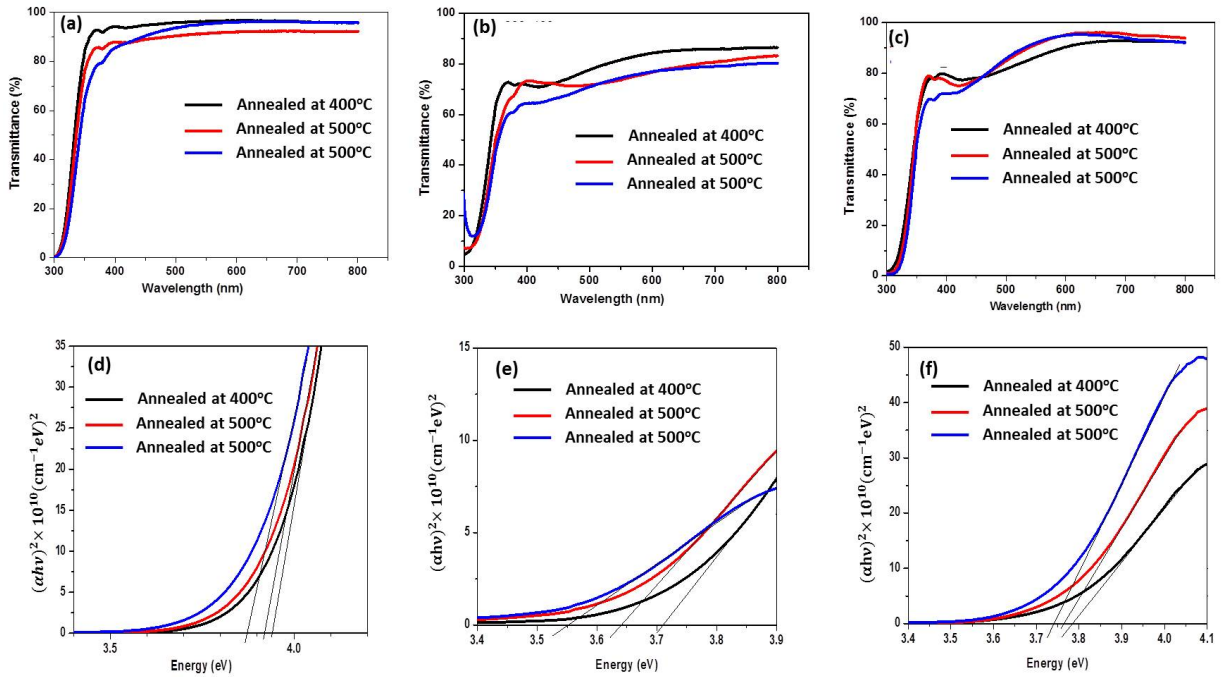


Figure 5: Transmittance spectra of the films dried at (a) 160 °C (b) 200 °C and (c) 250 °C; (d), (e), and (f) are Tauc's plot for the films respectively.

## 3.3. Electrical properties

Results of the measurement obtained from the linear four-point probe are shown in Table 1. Resistivity is a function of the concentration of carriers and mobility of carriers both of

10

which may be influenced by the presence of defects. In the thin films, the contribution of each of these factors to the resistivity, depends on the temperatures at which they were processed. From Table 1, the resistivity of the films were observed to decrease as the drying temperature was increased. An increase in the annealing temperature from $400\,^{\circ}\text{C}$ to $500\,^{\circ}\text{C}$, caused the resistivity to decrease. Further increase in the temperature of annealing from $500\,^{\circ}\text{C}$ to $600\,^{\circ}\text{C}$ caused the resistivity to increase. The initial reduction in resistivity due to an increase in the annealing temperature could be ascribed to increase in the size of grains in the films which leads to a reduction in grain boundaries, thereby enhancing the mobility of carriers. Despite the further increase in the grain size while the temperature of annealing increases, the resistivity increases. This might be prompted by the reduction in the concentration of defects in the films as explained by Mooney *et al* [36] leading to a reduction in the number of charge carriers. Generally, the resistivity of the films varies with both drying and annealing temperatures. At a low temperature of annealing, the resistivity depends on the mobility of carriers, at a higher temperature, resistivity is determined by the concentration of defects.

## 4. Conclusions

There was an improvement in the crystallinity of NiO films as annealing temperature increased. Films that were dried at $160\,^{\circ}\text{C}$ were not as crystalline as other films that were dried at higher temperatures. Films that were annealed at $300\,^{\circ}\text{C}$, irrespective of the drying temperatures, showed poor crystallinity. Morphology of the films revealed that they were homogeneous and consisting of grains of uniform size, the grain size increase from about 14 nm to 28 nm for films that were dried at $200\,^{\circ}\text{C}$ and 14 nm to 32 nm for films dried at $250\,^{\circ}\text{C}$ as the temperature of annealing was increased from $400\,^{\circ}\text{C}$ to $600\,^{\circ}\text{C}$. The transmittance of the films varied from 78% to 96%, from 64% to 87%, and from 72% to 92% as the wavelengths varied from 350 to 800 nm, for drying temperatures of $160\,^{\circ}\text{C}$, $200\,^{\circ}\text{C}$, and $300\,^{\circ}\text{C}$ respectively. Raman spectra of the films showed that two prominent Raman peaks at 558 cm$^{-1}$ and 1100 cm$^{-1}$ for one-phonon first-order longitudinal-optical (1P) LO mode and two-phonon second-order longitudinal-optical mode (2P) 2LO respectively were found

11

in all the films. For films that were dried at $250\,°C$ and annealed at $400\,°C$ and $500\,°C$, the enhancement of (1P) LO peak over that of (2P) 2LO was an indication that these films were richer in defects than those annealed at $600\,°C$. The electrical resistivity of the films as measured using the linear four-point probe system showed that the resistivity decreased with increasing drying temperature, the minimum resistivity was obtained in all the films at an annealing temperature of $500\,°C$. The resistivity of the films was found to depend on the grain size as well as the presence of defects. Annealing the films above $500\,°C$ reduced the concentration of defects and thus an increase in the resistivity was observed. This work revealed the dependence of resistivity of sol-gel fabricated NiO thin films on temperature of processing, both drying and annealing.

## References

[1] H. Sato, T. Minami, S. Takata, T. Yamada, Transparent conducting p-type NiO thin films prepared by magnetron sputtering, Thin Solid Films 236 (1-2) (1993) 27–31. doi:10.1016/0040-6090(93)90636-4.

[2] A. A. Al-Ghamdi, M. S. Abdel-wahab, A. Farghali, P. Hasan, Structural, optical and photo-catalytic activity of nanocrystalline NiO thin films, Materials Research Bulletin 75 (2016) 71–77. doi:10.1016/j.materresbull.2015.11.027.

[3] D. Adler, J. Feinleib, Electrical and optical properties of narrow-band materials, Physical Review B 2 (8) (1970) 3112. doi:10.1103/PhysRevB.2.3112.

[4] W.-L. Jang, Y.-M. Lu, W.-S. Hwang, W.-C. Chen, Electrical properties of Li-doped NiO films, Journal of the European Ceramic Society 30 (2) (2010) 503–508. doi:10.1016/j.jeurceramsoc.2009.05.041.

[5] S. Nandy, B. Saha, M. K. Mitra, K. Chattopadhyay, Effect of oxygen partial pressure on the electrical and optical properties of highly (200) oriented p-type $Ni_{1-x}O$ films by DC sputtering, Journal of Materials Science 42 (14) (2007) 5766–5772. doi:10.1007/s10853-006-1153-x.

[6] M. Kitao, K. Izawa, K. Urabe, T. Komatsu, S. Kuwano, S. Yamada, Preparation and electrochromic properties of RF-sputtered NiOx films prepared in $Ar/O_2/H_2$ atmosphere, Japanese Journal of Applied Physics 33 (12R) (1994) 6656. doi:10.1143/JJAP.33.6656.

[7] C.-Y. Lee, C.-M. Chiang, Y.-H. Wang, R.-H. Ma, A self-heating gas sensor with integrated NiO thin-film for formaldehyde detection, Sensors and Actuators B: Chemical 122 (2) (2007) 503–510. doi:10.1016/j.snb.2006.06.018.

[8] K. X. Steirer, J. P. Chesin, N. E. Widjonarko, J. J. Berry, A. Miedaner, D. S. Ginley, D. C. Olson, Solution deposited NiO thin-films as hole transport layers in organic photovoltaics, Organic Electronics 11 (8) (2010) 1414–1418. doi:10.1016/j.orgel.2010.05.008.

[9] J. R. Manders, S.-W. Tsang, M. J. Hartel, T.-H. Lai, S. Chen, C. M. Amb, J. R. Reynolds, F. So, Solution-processed nickel oxide hole transport layers in high efficiency polymer photovoltaic cells, Advanced Functional Materials 23 (23) (2013) 2993–3001. doi:10.1002/adfm.201202269.

[10] J. H. Kim, P.-W. Liang, S. T. Williams, N. Cho, C.-C. Chueh, M. S. Glaz, D. S. Ginger, A. K.-Y. Jen, High-performance and environmentally stable planar heterojunction perovskite solar cells based on a solution-processed copper-doped nickel oxide hole-transporting layer, Advanced Materials 27 (4) (2015) 695–701. doi:10.1002/adma.201404189.

[11] J.-M. Choi, S. Im, Ultraviolet enhanced Si-photodetector using p-NiO films, Applied Surface Science 244 (1-4) (2005) 435–438. doi:10.1016/j.apsusc.2004.09.152.

[12] S.-Y. Tsai, M.-H. Hon, Y.-M. Lu, Fabrication of transparent p-NiO/n-ZnO heterojunction devices for ultraviolet photodetectors, Solid-State Electronics 63 (1) (2011) 37–41. doi:10.1016/j.sse.2011.04.019.

[13] S.-W. Park, J.-M. Choi, E. Kim, S. Im, Inverted top-emitting organic light-emitting diodes using transparent conductive NiO electrode, Applied Surface Science 244 (1-4) (2005) 439–443. doi:10.1016/j.apsusc.2004.10.099.

[14] S. Wahyuningsih, C. Purnawan, T. E. Saraswati, E. Pramono, A. H. Ramelan, S. Pramono, A. Wisnugroho, Visible light photoelectrocatalytic degradation of rhodamine B using $Ti/TiO_2$-NiO photoanode, Journal of Environmental Protection 5 (17) (2014) 1630. doi:10.4236/jep.2014.517154.

[15] K. Patel, M. Desai, C. Panchal, B. Rehani, p-type transparent NiO thin films by e-beam evaporation techniques, Journal of Nano-and Electronic Physics 3 (1) (2011) 376.

[16] H.-L. Chen, Y.-M. Lu, W.-S. Hwang, Characterization of sputtered NiO thin films, Surface and Coatings Technology 198 (1-3) (2005) 138–142. doi:10.1016/j.surfcoat.2004.10.032.

[17] I. Porqueras, E. Bertran, Electrochromic behaviour of nickel oxide thin films deposited by thermal evaporation, Thin Solid Films 398 (2001) 41–44. doi:10.1016/S0040-6090(01)01301-3.

[18] D. Franta, B. Negulescu, L. Thomas, P. R. Dahoo, M. Guyot, I. Ohlídal, J. Mistrík, T. Yamaguchi, Optical properties of NiO thin films prepared by pulsed laser deposition technique, Applied Surface Science 244 (1-4) (2005) 426–430. doi:10.1016/j.apsusc.2004.09.150.

[19] A. Al-Ghamdi, W. E. Mahmoud, S. Yaghmour, F. Al-Marzouki, Structure and optical properties of nanocrystalline NiO thin film synthesized by sol–gel spin-coating method, Journal of Alloys and Com-

pounds 486 (1-2) (2009) 9–13. doi:10.1016/j.jallcom.2009.06.139.

[20] M. Jlassi, I. Sta, M. Hajji, H. Ezzaouia, Optical and electrical properties of nickel oxide thin films synthesized by sol–gel spin coating, Materials Science in Semiconductor Processing 21 (2014) 7–13. doi:10.1016/j.mssp.2014.01.018.

[21] M. Martini, G. Brito, M. Fantini, A. Craievich, A. Gorenstein, Electrochromic properties of NiO-based thin films prepared by sol–gel and dip coating, Electrochimica Acta 46 (13-14) (2001) 2275–2279. doi:10.1016/S0013-4686(01)00396-6.

[22] M. Ristova, J. Velevska, M. Ristov, Chemical bath deposition and electrochromic properties of $NiO_x$ films, Solar Energy Materials and Solar Cells 71 (2) (2002) 219–230. doi:10.1016/S0927-0248(01)00061-7.

[23] R. A. Ismail, S. Ghafori, G. A. Kadhim, Preparation and characterization of nanostructured nickel oxide thin films by spray pyrolysis, Applied Nanoscience 3 (6) (2013) 509–514. doi:10.1007/s13204-012-0152-2.

[24] P. Shankar, J. B. B. Rayappan, Gas sensing mechanism of metal oxides: The role of ambient atmosphere, type of semiconductor and gases - A review, Sci. Lett. J 4 (2015) 126.

[25] C. Garzella, E. Comini, E. Tempesti, C. Frigeri, G. Sberveglieri, $TiO_2$ thin films by a novel sol–gel processing for gas sensor applications, Sensors and Actuators B: Chemical 68 (1-3) (2000) 189–196. doi:10.1016/S0925-4005(00)00428-7.

[26] T. Schneller, R. Waser, M. Kosec, D. Payne, Chemical solution deposition of functional oxide thin films, Springer, 2013. doi:10.1007/978-3-211-99311-8.

[27] P. Baraldi, Thermal behavior of metal carboxylates: III-metal acetates, Spectrochimica Acta Part A: Molecular Spectroscopy 38 (1) (1982) 51–55. doi:10.1016/0584-8539(82)80176-1.

[28] I. Sta, M. Jlassi, M. Hajji, H. Ezzaouia, Structural, optical and electrical properties of undoped and Li-doped NiO thin films prepared by sol–gel spin coating method, Thin Solid Films 555 (2014) 131–137. doi:10.1016/j.tsf.2013.10.137.

[29] S. Akinkuade, B. Mwankemwa, J. Nel, W. Meyer, Structural, optical and electrical characteristics of nickel oxide thin films synthesised through chemical processing method, Physica B: Condensed Matter 535 (2018) 24–28. doi:10.1016/j.physb.2017.06.021.

[30] G. Zhang, L. Yu, H. E. Hoster, X. W. D. Lou, Synthesis of one-dimensional hierarchical NiO hollow nanostructures with enhanced supercapacitive performance, Nanoscale 5 (3) (2013) 877–881. doi:10.1039/c2nr33326k.

[31] S. Shariffudin, M. Mamat, S. Herman, M. Rusop, Influence of drying temperature on the structural, optical, and electrical properties of layer-by-layer ZnO nanoparticles seeded catalyst, Journal of Nanomaterials 2012 (2012) 122. doi:10.1155/2012/359103.

14

[32] E. Cazzanelli, A. Kuzmin, G. Mariotto, N. Mironova-Ulmane, Study of vibrational and magnetic excitations in $Ni_cMg_{1-c}O$ solid solutions by Raman spectroscopy, Journal of Physics: Condensed Matter 15 (12) (2003) 2045. doi:10.1088/0953-8984/15/12/321.

[33] D. Raoufi, A. Taherniya, The effect of substrate temperature on the microstructural, electrical and optical properties of Sn-doped indium oxide thin films, The European Physical Journal Applied Physics 70 (3) (2015) 30302. doi:10.1051/epjap/2015150004.

[34] M. Sultan, N. Sultana, Analysis of reflectance and transmittance characteristics of optical thin film for various film materials, thicknesses and substrates, Journal of Electrical & Electronics 4 (3) (2015) 1. doi:10.4172/2332-0796.1000160.

[35] M. Singh, M. Goyal, K. Devlal, Size and shape effects on the band gap of semiconductor compound nanomaterials, Journal of Taibah University for Science 12 (4) (2018) 470–475. doi:10.1080/16583655.2018.1473946.

[36] J. B. Mooney, S. B. Radding, Spray pyrolysis processing, Annual Review of Materials Science 12 (1) (1982) 81–101. doi:10.1146/annurev.ms.12.080182.000501.